ACS APPLIED MATERIALS & INTERFACES

Research Article

www.acsami.org

Core-Double-Shell, Carbon Nanotube@Polypyrrole@MnO_2 Sponge as Freestanding, Compressible Supercapacitor Electrode

Peixu Li,[†] Yanbing Yang,[‡] Enzheng Shi,[§] Qicang Shen,[⊥] Yuanyuan Shang,[§] Shiting Wu,[§] Jinquan Wei,[⊥] Kunlin Wang,[⊥] Hongwei Zhu,[⊥] Quan Yuan,[‡] Anyuan Cao,*[,§] and Dehai Wu*[,†]

[†]Department of Mechanical Engineering, Tsinghua University, Beijing 100084, P. R. China

[‡]Key Laboratory of Analytical Chemistry for Biology and Medicine (Ministry of Education), College of Chemistry and Molecular Sciences, Wuhan University, Wuhan, Hubei 430072, China

[§]Department of Materials Science and Engineering, College of Engineering, Peking University, Beijing 100871, P. R. China

[⊥]Key Laboratory for Advanced Materials Processing Technology and School of Materials Science and Engineering, Tsinghua University, Beijing 100084, P. R. China

Supporting Information

ABSTRACT: Design and fabrication of structurally optimized electrode materials are important for many energy applications such as supercapacitors and batteries. Here, we report a three-component, hierarchical, bulk electrode with tailored microstructure and electrochemical properties. Our supercapacitor electrode consists of a three-dimensional carbon nanotube (CNT) network (also called sponge) as a flexible and conductive skeleton, an intermediate polymer layer (polypyrrole, PPy) with good interface, and a metal oxide layer outside providing more surface area. These three components form a well-defined core-double-shell configuration that is distinct from simple core-shell or hybrid structures, and the synergistic effect leads to enhanced supercapacitor performance including high specific capacitance (even under severe compression) and excellent cycling stability. The mechanism study reveals that the shell sequence is a key factor; in our system, the CNT−PPy−MnO_2 structure shows higher capacitance than the CNT−MnO_2−PPy sequence. Our porous core-double-shell sponges can serve as freestanding, compressible electrodes for various energy devices.

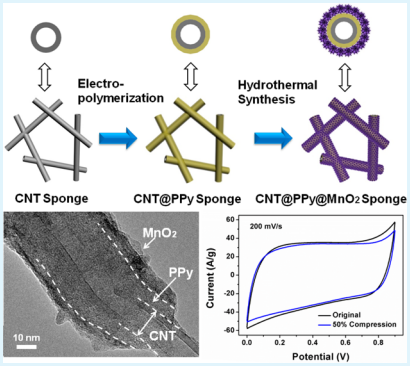

KEYWORDS: *carbon nanotube sponge, core-double-shell, supercapacitor, flexible electrode*

1. INTRODUCTION

Developing efficient energy storage systems such as supercapacitors and batteries demands rational design and controlled fabrication of bulk electrode materials.[1−6] Combining materials with different functions to form hybrid, hierarchical structures is an effective approach toward novel-design and high performance electrodes. This strategy has been explored in supercapacitors in which binary and ternary composite electrodes have been widely studied.[7−16] Specifically, amorphous carbon particles, carbon nanotubes (CNTs), or graphene forming conductive networks are combined with pseudo materials such as polymers and metal oxides to make a composite structure.[17−22] Previous study has demonstrated the synergistic effect produced by integrating multiple components, which could overcome the limitation of pseudo materials (e.g., low conductivity of metal oxides) and improve specific capacitance. In this regard, carbon materials-conducting polymers,[8,10,17,21,22] carbon materials-metal oxides,[9,18−20] conducting polymers-metal oxides,[11,23,24] and carbon materials-metal oxides-conducting polymers[13,25−30] have been fabricated and investigated for supercapacitor electrodes.

Although there have been several studies on ternary electrodes involving CNTs (graphene) and two types of pseudo materials, those electrodes do not exhibit a well-defined three-dimensional (3D) configuration and the composite structure is not well controlled.[13,25−30] Typically, CNTs were dispersed in solution and mixed with precursors for pseudo materials, and the hybrid structure was synthesized by appropriate treatments (thermal annealing).[13,26−29] Those products are generally in powder form in which aggregation of active materials would compromise the porosity and available surface area. More importantly, because CNTs were hybridized with pseudo materials first and then assembled into electrodes, it is difficult to create a highly conductive CNT network due to the presence of a pseudo material layer between CNTs (preventing direct inter-CNT contact). The mechanical strength and flexibility are not high, and binders are usually added in order to make freestanding electrodes. In addition, pseudo materials such as polymers and metal oxides are grafted

Received: January 26, 2014
Accepted: March 12, 2014
Published: March 12, 2014

onto CNTs as a mixture rather than individual layers,[25,27] making it less straightforward for mechanism study and structural optimization.

Here, we report a 3D porous hierarchical sponge electrode that can fully utilize the electrical conductivity of CNT networks and also has a synergistic effect from a combination of two pseudo materials with tailored structure. The hybrid structure is based on CNT sponges reported by our group, which have demonstrated supercapacitor properties as pristine and hybrid sponges.[31,32] The electrode is fabricated by direct deposition of pseudo materials into the porous sponge while protecting the original interconnected CNT network with high conductivity. A polymeric and metal oxide pseudo material was selected, respectively, creating a macroscopic CNT@PPy@MnO_2 (PPy is polypyrrole) core-double-shell sponge with good flexibility (allowing severe compression without collapse). The core-double-shell skeleton is the most important feature here (also distinct from previous simple core-shell structures) that is responsible for high capacitance, and the shell sequence (PPy outside or MnO_2 outside) can be controlled to understand related mechanism and optimize electrode configuration. Also, the ternary hybrid sponges maintain stable characteristics under large degree compression with improved volume-normalized capacitance. Our core-double-shell sponges represent a possible route toward high performance electrodes with predefined configuration and controlled fabrication.

2. EXPERIMENTAL SECTION

2.1. Fabrication of CNT@PPy@MnO_2 Core-Double-Shell Sponges. CNT sponges were synthesized by chemical vapor deposition (CVD), as reported by our group previously. To fabricate the core-double-shell sponge, we first synthesized the CNT@PPy core-shell sponge by electropolymerization and then attached a MnO_2 shell through a hydrothermal process. An as-grown bulk CNT sponge block with edge size of several mm was immersed in Py/acetone solution with a concentration of 0.1 M for 0.5 h. Then, the CNT sponge with Py monomers adsorbed on the surface of each individual CNT was used as the working electrode under a potential of 0.8 V in 0.3 M $NaClO_4$ aqueous solution. The electropolymerization of Py was performed in a three-electrode electrochemical workstation (CHI660D instruments, Shanghai, China). A Pt wire and Ag/AgCl were used as the counter and reference electrodes, respectively. After a typical electropolymerization time of 10 minutes, the CNT@PPy core-shell sponge was obtained. The PPy loading can be controlled by the Py concentration in acetone and the absorption period. In the hydrothermal process, 0.02 mol/L $KMnO_4$ solution was firstly prepared and the pH value of the solution was adjusted by slowly adding sulfuric acid to pH = 1. The obtained CNT@PPy sponge was immersed in the $KMnO_4$ solution, further stirred for 30 s, and then transferred into a Teflon-lined stainless steel autoclave, sealed and maintained at 120 °C for 20 min. A MnO_2 shell was attached outside the PPy shell. The resulting sponge was rinsed with distilled water and then freeze-dried to maintain the porous structure.

2.2. Material Characterization. The sample morphology and structure were characterized using scanning electron microscopy (SEM, LEO 1530), transmission electron microscopy (TEM, JEOL 2010), and an X-ray diffraction (XRD) spectroscope (Bruker-D8 Discover). FTIR spectra were recorded on a FTIR system (Bruker Vector22). X-ray photoelectron spectroscopy (XPS) was performed using an ESCALAB 250Xi spectrometer. Raman spectra were recorded using a RM 2000 Microscopic Confocal Raman Spectrometer (Renishaw PLC, England) with a 633 nm laser. Thermogravimetric analysis (TGA) was conducted on a TGA Q5000 analyzer from 30 to 800 °C under air at a heating rate of 20 °C min^{-1}. Mechanical tests were carried out by a single-column static instrument (Instron 5843) equipped with two flat-surface compression stages and a 10 N load cell. The N_2 adsorption and desorption isotherms were measured at 77 K in a liquid nitrogen bath using a QUANTACHROME Autosorb-iQ analyzer. The BET specific surface area of sponges was measured. The pore volume and pore size distribution were obtained using the Barrett–Joyner–Halenda (BJH) method.

2.3. Electrochemical Measurements. The electrochemical properties of the sponge including cyclic voltammetry (CV), galvanostatic charge/discharge, and electrochemical impedance spectroscopy (EIS) were measured using a CHI660D electrochemical workstation in a three-electrode configuration. The sponge clamped by two polymeric blocks in original state (no compression) or at predefined compressive strains was used as working electrode. Platinum wire twisted around the polymeric clamp and connected to the sponge electrode was used as the current collector. A platinum wire and a saturated calomel electrode (SCE) were used as counter and reference electrodes, respectively. The CV curves were measured under different scan rates of 2–200 mV/s between 0 and 0.9 V. EIS measurements were carried out in the frequency range from 100 kHz to 0.01 Hz at open circuit potential with an ac perturbation of 5 mV. Electrochemical measurements were carried out in a 2 M KCl aqueous electrolyte at room temperature. The specific capacitance of the sponge electrode (C_S) was calculated from the CV curves and discharging curves according to eqs 1 and 2, respectively.

$$C_S = \int \frac{I}{m} dV / \nu \Delta V \tag{1}$$

$$C_S = \frac{I \Delta t}{m \Delta U} \tag{2}$$

where I is the response current (A), m is the total mass the sponge electrode (including CNTs, MnO_2, and PPy) (g), ΔV is the potential range in the CV (V), ν is the potential scan rate (mV/s), ΔU is the potential window in the discharging process, and Δt is the discharging time.

3. RESULTS AND DISCUSSION

Our method involved two hybridization steps, in which a porous CNT sponge was immersed in precursor solutions to deposit different pseudo materials sequentially in a controlled manner, as illustrated in Figure 1 (see Experimental Section for details). First, a uniform PPy layer was coated onto the CNT surface throughout the sponge by electropolymerization,

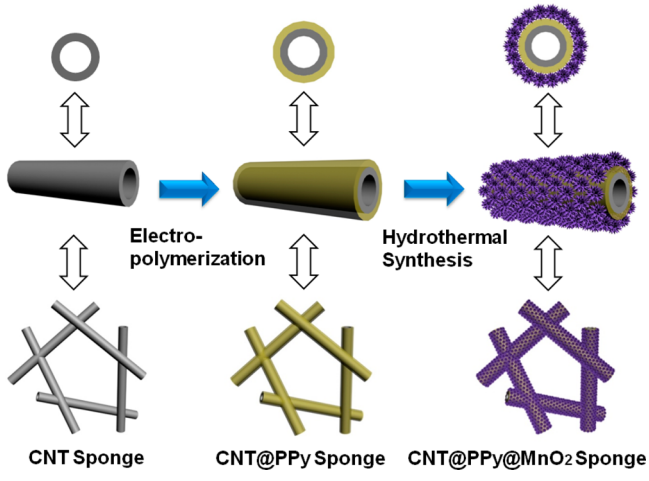

Figure 1. Schematic for the fabrication process from CNT sponge to CNT@PPy@MnO_2 core-double-shell sponge. A uniform PPy layer was firstly coated on the surface of individual CNTs by electropolymerization to produce an intermediate CNT@PPy core-shell sponge. Then, through a hydrothermal process, a MnO_2 shell was attached outside the PPy shell, leading to the formation of the core-double-shell CNT@PPy@MnO_2 sponge.

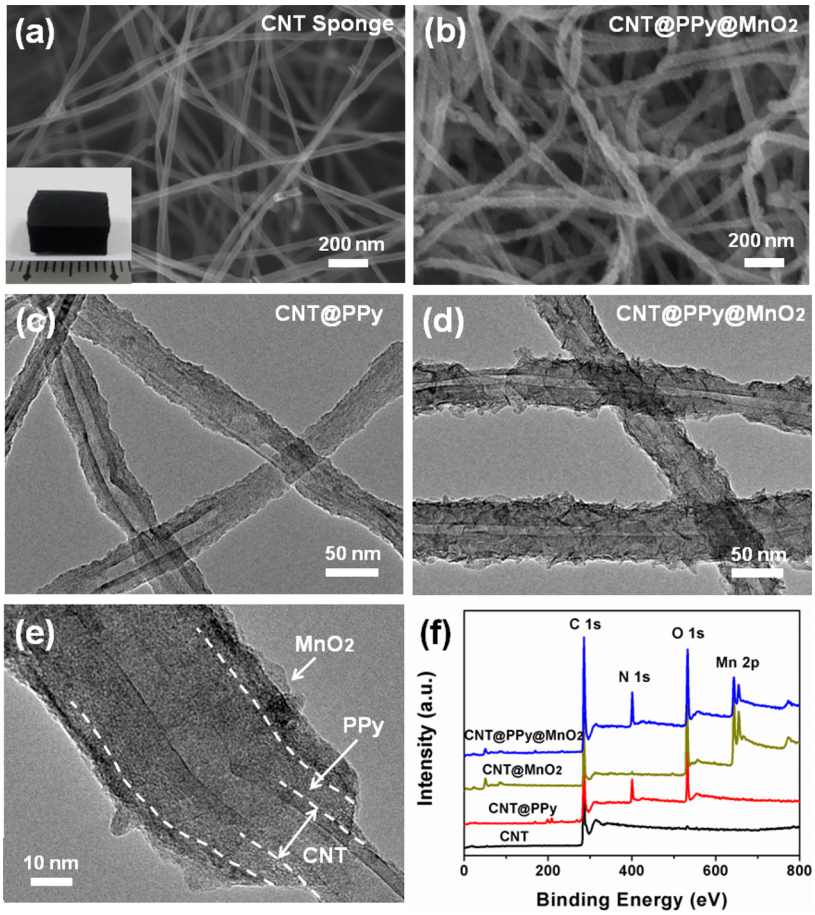

Figure 2. Characterization of CNT and core-double-shell sponges. (a) Cross-sectional SEM image of the CNT sponge. Inset shows a sponge block with edge size of several mm. (b) SEM image of the CNT@PPy@MnO_2 sponge. (c) TEM image of the CNT@PPy sponge. (d) TEM image of the CNT@PPy@MnO_2 sponge. (e) High-magnification TEM image showing the core-double-shell structure. (f) Surface scanning XPS full spectrum showing signals from Mn, O, N, and C elements in the CNT@PPy@MnO_2 sponge, compared with other sponges.

forming a binary CNT@PPy sponge. Second, a MnO_2 layer was attached to the PPy shell by a low temperature hydrothermal process, resulting in a ternary CNT@PPy@MnO_2 sponge with increased hierarchy. Because all CNTs were completely immersed in precursor solutions, the PPy and MnO_2 layers wrapped the entire surface of each nanotube nicely so that a core-double-shell structure formed. Our core-double-shell sponges have three distinct features compared to previous hybrid materials: (1) Uniform PPy and MnO_2 layers with controlled thickness and mass loading can be coated throughout the sponge. A reversed shell sequence, CNT@MnO_2@PPy also can be obtained by first depositing MnO_2 (as inside shell) and then PPy (outside). (2) The original CNT network (including the inter-CNT junctions) was embedded within the pseudo material layers so that the electrical conductivity is preserved at maximum. (3) At a relatively thin coating thickness, the resulting core-double-shell sponge could maintain much porosity and flexibility of original CNT sponges. The CNT@MnO_2@PPy sponge can be compressed to large strains due to the presence of a robust CNT skeleton. These are favorable structural factors for supercapacitor applications.

We have characterized the structure of CNT and CNT@PPy@MnO_2 sponges by SEM and TEM. An as-synthesized CNT sponge (inset of Figure 2a) consists of a 3D network of randomly overlapped nanotubes, creating an open porous structure (Figure 2a). These are multi-walled CNTs with diameters of 20−50 nm and lengths up to tens of micrometers.[33] Such porous structure is favorable for depositing active materials by electropolymerization and hydrothermal processes, as the precursor solution could easily infiltrate into the inner portion of a bulk sponge through the empty space between CNTs. After grafting PPy and MnO_2, the CNTs are wrapped by a uniform shell and the average outer diameter has increased from about 25 nm (clean nanotubes) to 55 nm (with PPy and MnO_2) (Figure 2b). The original CNT network is well preserved, and the CNT@PPy@MnO_2 sponge remains highly porous. SEM images of a CNT@PPy and CNT@MnO_2 sponge show distinct morphologies after coating PPy or MnO2, respectively (Supporting Information, Figure S1).

TEM images of products at different stages (CNT@PPy and CNT@PPy@MnO_2, respectively) clearly reveal the structure evolution during hybridization. For the CNT@PPy core-shell sponge, there is a PPy layer (thickness of 10−20 nm) coated on the surface of individual CNTs (Figure 2c). In comparison, CNT surfaces within the CNT@PPy@MnO_2 sponge become rough due to the outside MnO_2 layer (Figure 2d), which usually exists as protruding nanosheets as reported before.[25,28] The diameters of the CNT@PPy@MnO_2 units are further increased to 60−80 nm. An enlarged view of a particular region clearly shows the core-double-shell structure consisting of a CNT inside, a PPy layer in the middle, and a MnO_2 layer at the outside; both shells have thicknesses of about 10 nm (Figure

dx.doi.org/10.1021/am500579c | ACS Appl. Mater. Interfaces 2014, 6, 5228−5234

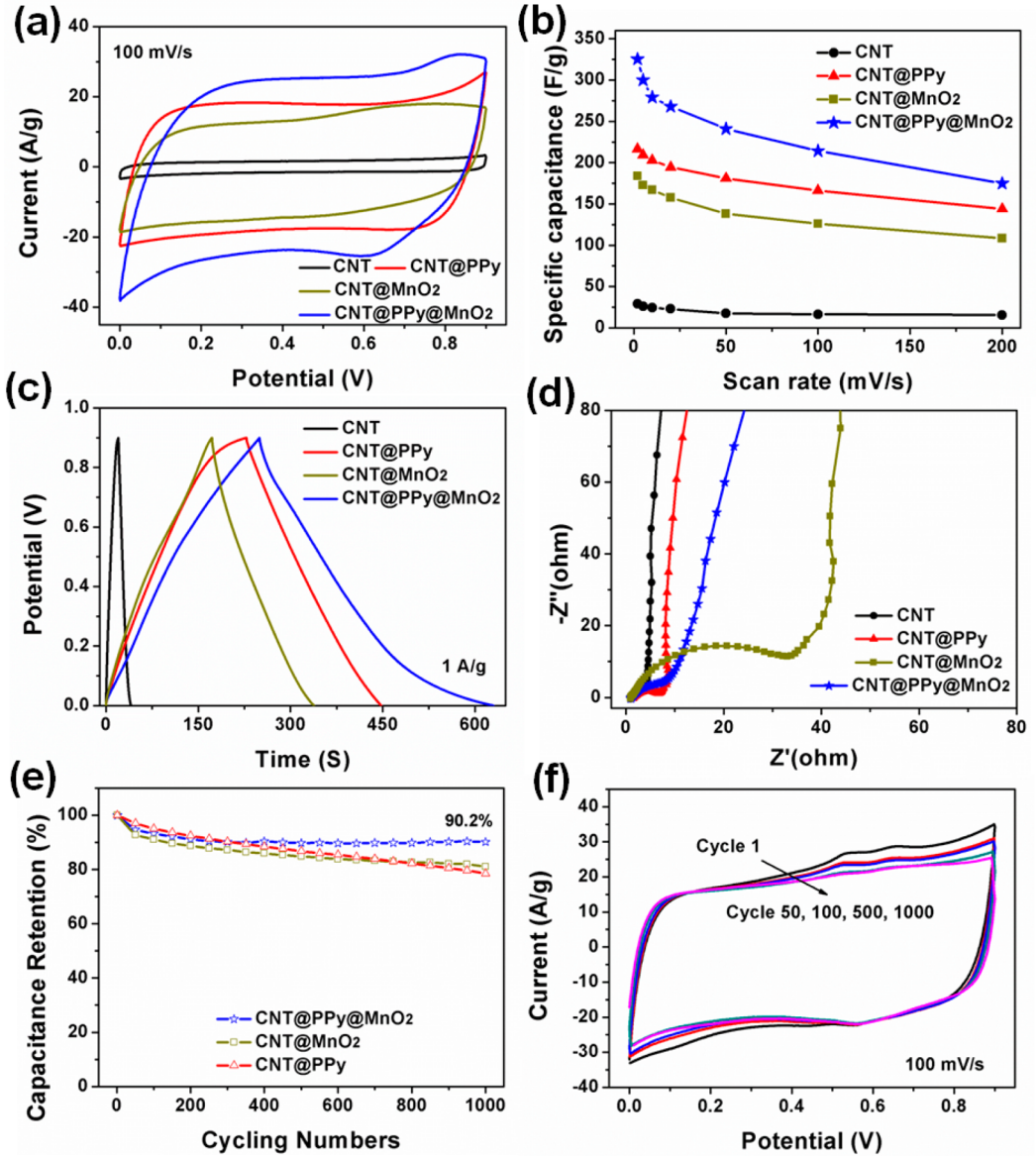

Figure 3. Supercapacitor application of CNT@PPy@MnO_2 core-double-shell sponges. (a) CV curves of the CNT, CNT@PPy, CNT@MnO_2, and CNT@PPy@MnO_2 sponges at a scan rate of 100 mV/s. (b) Calculated specific capacitances of the four types sponges at different scan rates. (c) Galvanostatic charge/discharge curves of the four sponges at a current of 0.5 A/g. (d) Nyquist plots of the EIS for the four sponges. (e) Cycling tests showing a better stability of CNT@PPy@MnO_2 sponge than CNT@PPy and CNT@MnO_2 sponges after 1000 charging and discharging cycles at 100 mV/s. (f) CV curves of cycle 1^{st}, 50^{th}, 100^{th}, 500^{th}, and 1000^{th} for the CNT@PPy@MnO_2 sponge.

2e). The CNT and its two shells have good interfaces (without cracks or holes), which ensures efficient charge transport along the radial direction from the outer shells to the CNT. Due to the strong adhesion of PPy to CNT by electropolymerization and the chemical connection between PPy and MnO_2, the PPy layer also serves as an intermediate layer for anchoring MnO_2 nanosheets, which otherwise could easily detach from the smooth CNT surface. Strong adhesion of pseudo materials to the CNT network is important for making stable supercapacitor electrodes. In addition, the rough MnO_2 shell also leads to increased specific surface area (108 m^2/g) in the hybrid sponge compared to the original CNT sponge (80 m^2/g), as well as increased percentage of pores with sizes in the range of 1.5−100 nm (accessible by liquid electrolyte) (Supporting Information, Figure S2).

Surface elemental analysis was carried out by XPS on the original and different hybrid sponges. The full XPS spectrum of a CNT@PPy@MnO_2 sponge reveals signals from Mn, O, N, and C elements, while there is only a C1s peak of an original CNT sponge (Figure 2f). Consistently, we observe N1s peak in a CNT@PPy sponge and Mn 2p peak in CNT@MnO2. The high-resolution Mn 2p core level spectra of CNT@PPy@MnO_2 and CNT @MnO_2 sponges show that Mn $2p_{3/2}$ and Mn $2p_{1/2}$ (having binding energies centered at 642.5 and 654.3 eV, respectively, with a spin energy separation of 11.8 eV) are in agreement with the reported data for MnO_2 (Supporting Information, Figure S3a).[29,30] We also studied the hybrid sponge structure by other characterization techniques including FTIR, XRD, Raman spectra, and TGA. The FTIR test results further verify the presence of PPy in the CNT@PPy@MnO_2 sponge. The peaks at ca. 1500 and 1455 cm^{-1} in the CNT@PPy@MnO_2 sample can be attributed to C−C and C−N stretching vibrations in the pyrrole ring, respectively (Supporting Information, Figure S3b). The CNT@PPy@MnO_2 sponge

dx.doi.org/10.1021/am500579c | ACS Appl. Mater. Interfaces 2014, 6, 5228−5234

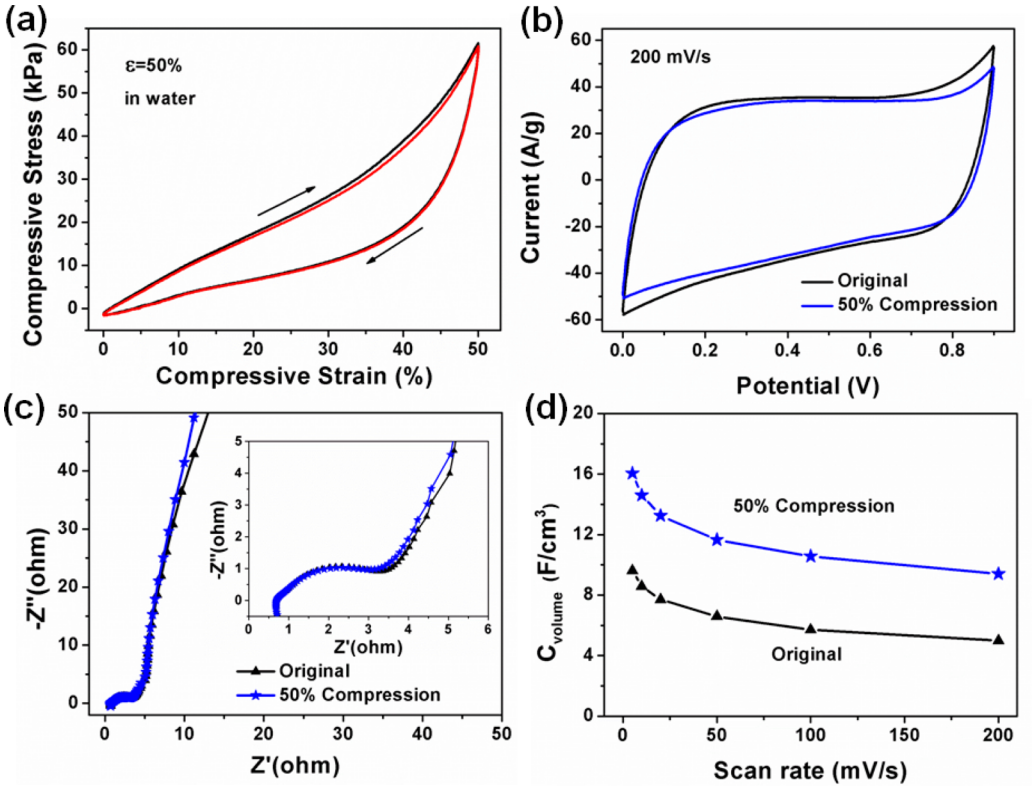

Figure 4. Supercapacitor performance under compression. (a) Mechanical testing (compressive stress-strain curves) of a CNT@PPy@MnO_2 sponge immersed in water and compressed to a strain of 50% for two cycles. The unloading curve shows elastic recovery. (b) CV curves of a CNT@PPy@MnO_2 sponge in original and compressed states (ε = 50%) at 200 mV/s. (c) Nyquist plots of the EIS for the sponge in original and compressed states. Inset is the magnification of Warburg semicircles from the spectra. (d) Volume-normalized capacitances (C_{volume}) of the sponge in original and compressed states at different scan rates.

shows a characteristic peak at 37.5° (although relatively weak) in the XRD pattern, indicating the presence of MnO_2 probably in an amorphous nature (Supporting Information, Figure S3c), which is favorable for supercapacitor applications.[34] Raman and TGA results also confirm the presence of MnO_2 (Raman peak at 480−680 cm^{-1}) and PPy (causing early weight loss when heated to about 100 °C) (Supporting Information, Figure S3d,e).

In order to evaluate the electrochemical performance of the as-prepared freestanding CNT@PPy@MnO_2 core-double-shell sponge, cyclic voltametry (CV), galvanostatic charge/discharge, and electrochemical impedance spectroscopy (EIS) measurements in a three-electrode system were employed. The electrolyte is 2M KCl aqueous solution. Figure 3a compares the CV curves of the CNT@PPy@MnO_2, CNT@PPy, CNT@MnO_2, and CNT sponge electrodes at a same scan rate of 100 mV/s. The mass content of MnO_2 and PPy in the hybrid sponges are ∼40 and ∼20 wt %, respectively. Detailed mass content for the hybrid sponge samples is shown in the Supporting Information, Table S1. The CV curves exhibit good rectangular and symmetric shapes, suggesting fast reversible Faradic reactions and ideal capacitive behavior. The PPy and MnO_2 functionalization leads to higher current density and enlarged area enclosed by the charging/discharging curves, with a specific capacitance (at 100 mV/s) increasing from 16.4 F/g (for CNT sponge) to 126.1 F/g for CNT@MnO_2, 166.3 F/g for CNT@PPy, and 214.2 F/g for CNT@PPy@MnO_2 sponge, respectively. The specific capacitance is calculated on the basis of the total hybrid sponge weight (CNTs and the active materials). Furthermore, the CNT@PPy@MnO_2 sponge shows a stable shape as the scan rate increased from 2 to 200 mV/s (Supporting Information, Figure S4). It reveals good rate performance, especially at large charge/discharge current densities. We have optimized the MnO_2 mass loading by controlling the hydrothermal synthesis period. The optimized synthesis period is 20 min with corresponding MnO_2 loading of ca. 39.1 wt % (Supporting Information, Figure S5). The highest capacitance is ca. 325 F/g obtained in the CNT@PPy@MnO_2 sponge at a scan rate of 2 mV/s, in contrast to 29.3 F/g for CNT sponge, 183.7 F/g for CNT@MnO_2, and 216.3 F/g for CNT@PPy, respectively (Figure 3b).This performance improvement is attributed to the synergistic effect of the high pseudo-capacitance of the conformal PPy and MnO_2 coating and the porous structure of CNT network. In the CNT@PPy@MnO_2 sponge, the inter CNTs provide a porous structure and a conductive network. The MnO_2 layer is mainly responsible for pseudo reactions; the middle PPy layer can improve the interaction between the outer MnO_2 layer and the inter CNTs, reduce the interface resistance, and improve the charge transfer. Figure 3c shows the galvanostatic charge/discharge curves at a constant current density of 1 A/g. The symmetrical triangle curves indicate good reversibility of the CNT@PPy@MnO_2 core-double-shell sponge electrode. Additionally, negligible voltage drop (IR drop) can be seen from the curve, indicating a really low internal resistance which is important for energy electrodes. We have also carried out the two-electrode configuration test by assembling the core-double-shell sponges into a prototype two-electrode symmetrical supercapacitor in 2M KCl aqueous electrolyte (Supporting Information, Figure S6). The sponge shows good rate performance, even under a

high scan rate of 1000 mV/s and a high charge/discharge current density of 50A/g. The highest specific capacitance of the electrode is 305.9 F/g at a scan rate of 2 mV/s (Supporting Information, Figure S6c). The maximum energy density and power density are 8.6 Wh/kg and 16.5 KW/kg, respectively (Supporting Information, Figure S6d).

The EIS test is conducted for further characterizing the CNT@PPy@MnO_2 electrode. Figure 3d shows the resulting Nyquist plots of the EIS spectra for the CNT@PPy@MnO_2, CNT@PPy, CNT@MnO_2, and CNT sponge electrodes. All spectra are composed of a typical semicircle in the high frequency region and a straight line at low frequency. The intercept of the semicircle on the real axis at high frequency represents the equivalent series resistance (R_s), and the diameter of the semicircle corresponds to the charge-transfer resistance (R_{ct}) of the electrode.[20] The R_s of the hybrid sponge electrodes are approximate (~1.0 Ω). However, the CNT@PPy@MnO_2 sponge electrode shows an obvious decrease of R_{ct} than that of the CNT@MnO_2 sponge electrode. This indicates that the middle PPy shell can improve the interaction between the outer MnO_2 nanosheets shell and the CNTs in the CNT@PPy@MnO_2 sponge, rendering electron transport from MnO_2 to CNTs more efficient. Cycling stability of the CNT@PPy@MnO_2 electrode has been investigated at a scan rate of 100 mV/s for 1000 charging/discharging cycles. The CNT@PPy@MnO_2 electrode shows a capacitance retention of 90.2%, which is higher than CNT@MnO_2 (81.1%) and CNT@PPy (78.5%) (Figure 3e). The CV curves become almost identical after about 500 charging and discharging cycles, indicating good stability of our CNT@PPy@MnO_2 sponge electrode (Figure 3f).

To further demonstrate the structure advantage of CNT@PPy@MnO_2, a CNT@MnO_2@PPy sponge with reversed shell sequence was fabricated by changing the order of the two synthesis processes. The CNT@MnO_2@PPy sponge also has a core-double-shell configuration but with PPy outside. We compared the supercapacitor performance of the two ternary hybrid sponges with similar PPy and MnO_2 loadings (Supporting Information, Figure S7). The CNT@MnO_2@PPy sponge shows a lower capacitance (241 F/g) than the CNT@PPy@MnO_2 sponge (325 F/g) (Supporting Information, Figure S7c). In particular, the R_{ct} of the CNT@MnO_2@PPy sponge is much higher than the CNT@PPy@MnO_2 sponge (Supporting Information, Figure S7d). We also compare another set of ternary hybrid sponge samples with more MnO_2 loading (ca. 58 wt %). The CNT−PPy−MnO_2 structure sequence also shows better performance than the CNT−MnO_2−PPy sequence (Supporting Information, Figure S8). This demonstrates that, in our CNT−PPy−MnO_2 ternary hybrid sponge, the core-double-shell structure design will affect the electrochemical performance.

Besides the improvement of specific capacitance by forming PPy and MnO_2 double shells, the CNT@PPy@MnO_2 sponge also can work under large degree compression. Figure 4a shows that the sponge can be immersed in water and compressed elastically. Two loading and unloading cycles show full thickness (volume) recovery by water absorption, which accompanies the fast sponge expansion to the original volume owing to the robust and elastic CNT network. We measured the supercapacitor performance of the same sponge in the original state and under *in situ* compression performed by specially designed clamps (Supporting Information, Figure S9). The sponge exhibits similar CV characteristics at a compressive strain of 50% compared with the original state (Figure 4b). Even when its volume has been greatly reduced, the sponge still retains more than 90% of the original specific capacitance. Since the 3D CNT network sustains an open porous and stable structure even under high compressive strain, liquid electrolyte can readily infiltrate and access the inner part of the compressed sponge, which is important for ion diffusion and minimizing capacitance loss. The galvanostatic charge/discharge tests of the original and compressed sponge are consistent with their CV results (Supporting Information, Figure S10). Under a high compressive strain (50%), the charge/discharge curve of the sponge maintains a symmetrical shape. The EIS of the CNT@PPy@MnO_2 sponge is shown in Figure 4c. The CNT@PPy@MnO_2 sponge shows similar Nyquist plots in original and compressed states (ε = 50%), indicating a stable ESR (~0.70 Ω) under compression. We further calculate the volume-normalized specific capacitance (C_{volume}), and in this case, the compressed sponge shows significantly improved C_{volume} because of large volume reduction. For example, at a scan rate of 5 mV/s, the C_{volume} value reaches 16.1 F/cm^3 under 50% compression, showing ca. 67% increase compared to the original sponge (9.6 F/cm^3) (Figure 4d). This result indicates it is possible to fabricate a compressible supercapacitor with enhanced volume-normalized capacitance.

4. CONCLUSION

In summary, we demonstrated a three-component CNT@PPy@MnO_2 sponge electrode with a distinct core-double-shell structure. Pseudo material layers with controlled thickness and shell sequence were coated uniformly throughout the CNT sponge, maintaining the original CNT network and interconnection. Synergistic effect from respective components (PPy and MnO_2) plus the porous conductive CNT network offers the hybrid sponge a superior electrochemical performance. The 3D CNT network can significantly reduce the internal resistance of the electrode and maintain the structure stability. Porous CNT@PPy@MnO_2 sponges can serve as freestanding, compressible electrodes for supercapacitors and other energy devices. Our core-double-shell structure may be applied to other electrochemical materials for design and fabrication of hybrid and hierarchical electrodes.

■ ASSOCIATED CONTENT

Ⓢ Supporting Information

The characterizations of the core-double-shell sponge, including XRD, Raman, TGA, nitrogen sorption isotherms, and pore size distribution. Supercapacitor performance comparison between the CNT@MnO_2@PPy and CNT@PPy@MnO_2 sponges. The supercapacitor performance of the CNT@PPy@MnO_2 sponge by the two-electrode configuration test. This information is available free of charge via the Internet at http://pubs.acs.org/.

■ AUTHOR INFORMATION

Corresponding Authors

*E-mail: anyuan@pku.edu.cn.
*E-mail: wdh-dme@tsinghua.edu.cn.

Notes

The authors declare no competing financial interest.

■ ACKNOWLEDGMENTS

This work was supported by the National Science Foundation of China (NSFC, grant numbers 91127004 and 51325202).

■ REFERENCES

(1) Zhang, L.; Zhao, X. Carbon-Based Materials as Supercapacitor Electrodes. *Chem. Soc. Rev.* **2009**, *38*, 2520−2531.
(2) Dai, L.; Chang, D.; Baek, J.; Lu, W. Carbon Nanomaterials for Advanced Energy Conversion and Storage. *Small* **2012**, *8*, 1130−1166.
(3) He, Y.; Chen, W.; Gao, C.; Zhou, J.; Li, X.; Xie, E. An Overview of Carbon Materials for Flexible Electrochemical Capacitors. *Nanoscale* **2013**, *5*, 8799−8820.
(4) Bordjiba, T.; Mohamedi, M.; Dao, L. New Class of Carbon-Nanotube Aerogel Electrodes for Electrochemical Power Sources. *Adv. Mater.* **2008**, *20*, 815−819.
(5) Liu, B.; Soares, P.; Checkles, C.; Zhao, Y.; Yu, G. Three-Dimensional Hierarchical Ternary Nanostructures for High-Performance Li-Ion Battery Anodes. *Nano Lett.* **2013**, *13*, 3414−3419.
(6) Yu, G.; Xie, X.; Pan, L.; Bao, Z.; Cui, Y. Hybrid Nanostructured Materials for High-Performance Electrochemical Capacitors. *Nano Energy* **2013**, *2*, 213−234.
(7) Lota, G.; Fic, K.; Frackowiak, E. Carbon Nanotubes and Their Composites in Electrochemical Applications. *Energy Environ. Sci.* **2011**, *4*, 1592−1605.
(8) Peng, C.; Zhang, S.; Jewell, D.; Chen, G. Carbon Nanotube and Conducting Polymer Composites for Supercapacitors. *Prog. Nat. Sci.* **2008**, *18*, 777−788.
(9) Wu, Z.; Zhou, G.; Yin, L.; Ren, W.; Li, F.; Cheng, H. Graphene/Metal Oxide Composite Electrode Materials for Energy Storage. *Nano Energy* **2012**, *1*, 107−131.
(10) Sun, Y.; Shi, G. Graphene/Polymer Composites for Energy Applications. *J. Polym. Sci., Part B: Polym. Phys.* **2013**, *51*, 231−253.
(11) Bahloul, A.; Nessark, B.; Briot, E.; Groult, H.; Mauger, A.; Zaghib, K.; Julien, C. M. Polypyrrole-Covered MnO_2 as Electrode Material for Supercapacitor. *J. Power Sources* **2013**, *240*, 267−272.
(12) Zhong, J.; Wang, A.; Li, G.; Wang, J.; Ou, Y.; Tong, Y. Co_3O_4/Ni(OH)(2) Composite Mesoporous Nanosheet Networks as a Promising Electrode for Supercapacitor Applications. *J. Mater. Chem.* **2012**, *22*, 5656−5665.
(13) Hou, Y.; Cheng, Y.; Hobson, T.; Liu, J. Design and Synthesis of Hierarchical MnO_2 Nanospheres/Carbon Nanotubes/Conducting Polymer Ternary Composite for High Performance Electrochemical Electrodes. *Nano Lett.* **2010**, *10*, 2727−2733.
(14) Liu, N.; Ma, W.; Tao, J.; Zhang, X.; Su, J.; Li, L.; Yang, C.; Gao, Y.; Golberg, D.; Bando, Y. Cable-Type Supercapacitors of Three-Dimensional Cotton Thread Based Multi-Grade Nanostructures for Wearable Energy Storage. *Adv. Mater.* **2013**, *25*, 4925−4931.
(15) Tao, J.; Liu, N.; Ma, W.; Ding, L.; Li, L.; Su, J.; Gao, Y. Solid-State High Performance Flexible Supercapacitors Based on Polypyrrole-MnO_2-Carbon Fiber Hybrid Structure. *Sci. Rep.* **2013**, *3*, 2286.
(16) Tao, J.; Liu, N.; Li, L.; Su, J.; Gao, Y. Hierarchical Nanostructures of Polypyrrole@MnO_2 Composite Electrodes for High Performance Solid-State Asymmetric Supercapacitors. *Nanoscale* **2014**, *6*, 2922−2928.
(17) Fan, L.; Hu, Y.; Maier, J.; Adelhelm, P.; Smarsly, B.; Antonietti, M. High Electroactivity of Polyaniline in Supercapacitors by Using a Hierarchically Porous Carbon Monolith as a Support. *Adv. Funct. Mater.* **2007**, *17*, 3083−3087.
(18) Hu, L.; Chen, W.; Xie, X.; Liu, N.; Yang, Y.; Wu, H.; Yao, Y.; Pasta, M.; Alshareef, H. N.; Cui, Y. Symmetrical MnO_2-Carbon Nanotube-Textile Nanostructures for Wearable Pseudocapacitors with High Mass Loading. *ACS Nano* **2011**, *5*, 8904−8913.
(19) Mao, L.; Zhang, K.; Chan, H. S. O.; Wu, J. Nanostructured MnO_2/Graphene Composites for Supercapacitor Electrodes: The Effect of Morphology, Crystallinity and Composition. *J. Mater. Chem.* **2012**, *22*, 1845−1851.
(20) Yu, G.; Hu, L.; Liu, N.; Wang, H.; Vosgueritchian, M.; Yang, Y.; Cui, Y.; Bao, Z. Enhancing the Supercapacitor Performance of Graphene/MnO_2 Nanostructured Electrodes by Conductive Wrapping. *Nano Lett.* **2011**, *11*, 4438−4442.
(21) Antiohos, D.; Folkes, G.; Sherrell, P.; Ashraf, S.; Wallace, G. G.; Aitchison, P.; Harris, A. T.; Chen, J.; Minett, A. I. Compositional Effects of PEDOT-PSS/Single Walled Carbon Nanotube Films on Supercapacitor Device Performance. *J. Mater. Chem.* **2011**, *21*, 15987−15994.
(22) Zhao, Y.; Liu, J.; Hu, Y.; Cheng, H.; Hu, C.; Jiang, C.; Jiang, L.; Cao, A.; Qu, L. Highly Compression-Tolerant Supercapacitor Based on Polypyrrole-Mediated Graphene Foam Electrodes. *Adv. Mater.* **2013**, *25*, 591−595.
(23) Nakayama, M.; Kashiwa, Y.; Suzuki, K. Electrochromic Properties of MnO_2-Based Layered Polymer Nanocomposite. *J. Electrochem. Soc.* **2009**, *156*, D125−D130.
(24) Lu, Q.; Zhou, Y. Synthesis of Mesoporous Polythiophene/MnO(2) Nanocomposite and Its Enhanced Pseudocapacitive Properties. *J. Power Sources* **2011**, *196*, 4088−4094.
(25) Wang, J.; Yang, Y.; Huang, Z.; Kang, F. Rational Synthesis of MnO_2/Conducting Polypyrrole@Carbon Nanofiber Triaxial Nano-Cables for High-Performance Supercapacitors. *J. Mater. Chem.* **2012**, *22*, 16943−16949.
(26) Yuan, C.; Su, L.; Gao, B.; Zhang, X. Enhanced Electrochemical Stability and Charge Storage of MnO_2/Carbon Nanotubes Composite Modified by Polyaniline Coating Layer in Acidic Electrolytes. *Electrochim. Acta* **2008**, *53*, 7039−7047.
(27) Sharma, R. K.; Karakoti, A.; Seal, S.; Zhai, L. Multiwall Carbon Nanotube-Poly(4-Styrenesulfonic Acid) Supported Polypyrrole/Manganese Oxide Nano-Composites for High Performance Electrochemical Electrodes. *J. Power Sources* **2010**, *195*, 1256−1262.
(28) Li, Q.; Liu, J.; Zou, J.; Chunder, A.; Chen, Y.; Zhai, L. Synthesis and Electrochemical Performance of Multi-Walled Carbon Nanotube/Polyaniline/MnO_2 Ternary Coaxial Nanostructures for Supercapacitors. *J. Power Sources* **2011**, *196*, 565−572.
(29) Kim, K.; Park, S. Synthesis and High Electrochemical Performance of Polyaniline/MnO_2-Coated Multi-Walled Carbon Nanotube-Based Hybrid Electrodes. *J. Solid State Electrochem.* **2012**, *16*, 2751−2758.
(30) Wang, G.; Tang, Q.; Bao, H.; Li, X.; Wang, G. Synthesis of Hierarchical Sulfonated Graphene/MnO_2/Polyaniline Ternary Composite and Its Improved Electrochemical Performance. *J. Power Sources* **2013**, *241*, 231−238.
(31) Li, P.; Kong, C.; Shang, Y.; Shi, E.; Yu, Y.; Qian, W.; Wei, F.; Wei, J.; Wang, K.; Zhu, H.; Cao, A.; Wu, D. Highly Deformation-Tolerant Carbon Nanotube Sponges as Supercapacitor Electrodes. *Nanoscale* **2013**, *5*, 8472−8479.
(32) Li, P.; Shi, E.; Yang, Y.; Shang, Y.; Peng, Q.; Wu, S.; Wei, J.; Wang, K.; Zhu, H.; Yuan, Q.; Cao, A.; Wu, D. CNT-Polypyrrole Core-Shell Sponge and Its Application as Highly Compressible Supercapacitor Electrode. *Nano Res.* **2013**, DOI: 10.1007/s12274-013-0388-5.
(33) Gui, X.; Wei, J.; Wang, K.; Cao, A.; Zhu, H.; Jia, Y.; Shu, Q.; Wu, D. Carbon Nanotube Sponges. *Adv. Mater.* **2010**, *22*, 617−621.
(34) Bao, S.; He, B.; Liang, Y.; Zhou, W.; Li, H. Synthesis and Electrochemical Characterization of Amorphous MnO_2 for Electrochemical Capacitor. *Mater. Sci. Eng., A: Struct. Mater. Prop. Microstruct. Process.* **2005**, *397*, 305−309.